Bedding Dips in CRP-2A, Victoria Land Basin, Antarctica

R.D. Jarrard[1], J. D. Brink[1], C. Bücker[2], T. Wonik[2], T. Wilson[3] & T. Paulsen[3]

[1]Dept. of Geology & Geophysics, 717 WBB, Univ. of Utah 135 S. 1460 East, Salt Lake City - UT 84112-0111 - USA
[2]GGA, Joint Scientific Research Institute Stilleweg 2, 30655 Hannover - Germany
[3]Dept. of Geological Sciences, Ohio State University 275 Mendenhall, 125 S. Oval Mall, Columbus - OH 43210 - USA

Corresponding author (jarrard@mail.mines.utah.edu)

Abstract - Bedding dips in the CRP-2A drillhole were determined in two ways: (1) analysis of a dipmeter log, and (2) identification of bed boundaries on digital images of the outer core surface. The two methods document the downhole increase in structural dip, to a maximum of 15° in the lowest 150 m of the hole. Dipmeter data, which are azimuthally oriented, indicate a 75° azimuth for structural tilting, in agreement with seismic reflection profiles. Core and log dips indicate that structural dip increases by 5-7° between 325 and 480 mbsf. Both, however, also exhibit high dip inhomogeneity because of depositional (*e.g.*, cross bedding) and post-depositional (*e.g.*, soft-sediment deformation) processes. This variability adds ambiguity to the search for angular unconformities within the CRP-2A drillhole. Dip directions of different lithologies are generally similar, as are dip directions for the four kinds of systems tracts. Downdip azimuths of sands and muds are slightly different from those of diamicts, possibly reflecting the divergence between ENE offshore dip and ESE glacial advance.
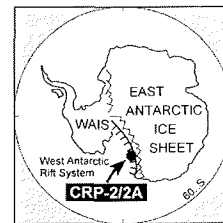
INTRODUCTION

The Cape Roberts Project (CRP) is an international drilling program whose aim is to reconstruct Neogene to Palaeogene palaeoclimate and tectonic history, by continuous coring and well logging at sites near Cape Roberts, Antarctica. The first CRP drillhole, CRP-1, obtained 148 metres of Quaternary and Miocene sediments (Cape Roberts Science Team, 1998). The second CRP drillhole, CRP-2/2A, extended to 624 metres below sea floor (mbsf) with an average 94% recovery of Oligocene to Quaternary sediments (Cape Roberts Science Team, 1999).

This study uses two data sources, whole-core images and dipmeter logs, to determine bedding dips in the CRP-2A drillhole. Digital whole-core images were obtained at the drill site (Cape Roberts Science Team, 1999), primarily for structural analyses (Wilson & Paulsen, this volume). Dipmeter logs are one of several kinds of downhole logs run at CRP-2A (Cape Roberts Science Team, 1999); processing and analyses of the other logs are presented by Brink & Jarrard (this volume), Brink et al. (this volume), Bücker et al. (this volume), and Moos et al. (this volume).

The studies of whole-core images and dipmeter logs presented here had three objectives: (1) extraction of a microresistivity log, (2) orientation of some cores, and (3) determination of sedimentary and structural dips. Dipmeter logging has a vertical resolution that is 1-2 orders of magnitude higher than other porosity-sensitive logging. As part of our dipmeter processing, we extract a microresistivity log that Brink & Jarrard (this volume) convert to porosity and that Brink et al. (this volume) interpret sedimentologically. Although the CRP-2A cores were not oriented with respect to North during data acquisition, later orientation is sometimes possible: dipmeter data provide bedding orientation, so recognition of the same bedding in whole-core images provides orientation for those images (Paulsen et al., this volume).

Although this paper provides a foundation for the microresistivity and core orientation objectives, its main goal is determination of sedimentary and structural dips. By determining bedding dips and azimuths throughout CRP-2A, we hoped to detect subtle angular unconformities and identify sedimentary dips that might provide clues to sedimentary facies (*e.g.*, cross bedding) or post-depositional processes (*e.g.*, slumping).

CORE DATA PROCESSING

As part of the core processing flow at Cape Roberts Drillsite, both whole cores and split cores were routinely digitally imaged with a DMT CoreScan color scanner (Cape Roberts Science Team, 1999). Prior to core splitting, the outer surfaces of most cores were imaged; exceptions were cores with too little strength to be rotated on the scanner without breaking up. After core splitting, the cut faces of all split cores were imaged; black-and-white copies of these images are included in the CRP Initial Reports (Cape Roberts Science Team, 1999). The core-image analyses reported here are confined to the whole-core images, because they provide true bedding dips, in contrast to the apparent dips evident on a split-core face.

Each whole-core scan, consisting of 10-100 cm of core, was saved as an individual digital file. Also evident on these color images are two orientation scribe lines, one red and one blue. Scribing is undertaken just before removal of the core from the core barrel, so it cannot account for rotations between adjacent core segments during the coring process. In many cases, it is possible to determine relative orientation among successive core pieces and among

successive core images, by matching and fitting together the broken core surfaces. This process does not have to be undertaken on the core itself. It can be done with the whole-core images in a process referred to as "stitching". Each interval of stitched-together images is a continuous composite with correct relative orientations among successive pieces. Twenty-seven intervals, totaling 126 m (22% of the recovered core), were stitched (Tab. 1). Many other intervals were stitchable but were not stitched because the process is so time consuming. Note, however, that this stitching does not orient the cores with respect to a geographic (NESW) coordinate system.

All the stitched core intervals of table 1 were included in our studies of bedding dips. In addition, we examined most of the unstitched whole-core scans. Selection of these latter zones was based in part on usefulness for core orienting: zones with oriented borehole televiewer log (Moos et al., this volume) and zones lacking dipmeter data were lower in priority. An additional selection criterion was proximity to angular unconformities: all images were examined in zones bracketing possible angular unconformities. Unstudied intervals consist mainly of the following: 170-195 mbsf, 200-240 mbsf, 340-390 mbsf, some cores in the interval 500-565 mbsf, and many cores above 130 mbsf.

Image processing and analysis for all images, stitched or unstitched, consisted of the following initial steps: (1) import the bitmap image into Adobe Photoshop; (2) convert the image from RGB color to grey levels; (3) adjust the grey-level scale, to obtain maximum resolution of any bedding that may be present. Rarely did we find that color was useful for detection of bedding, whereas grey-level adjustment was always useful: by zooming the grey-level spectrum to subdivide and concentrate on the majority of observed intensities in an image, initially obvious bedding is retained, and some bedding too subtle to resolve on the original image is revealed. "Bedding" is here defined as a change in grey level, sinusoidal in shape on these unwrapped 360° images, interpreted to be caused by a change in lithology or porosity. Fractures are readily distinguished from bedding within these images, and we exclude fractures from our analyses.

If no bedding is observed, processing of that image is terminated. Of the 40 stitched and 274 unstitched files examined, 133 had identifiable bedding. For each of these files, the following steps were undertaken: (1) sampling density was reduced from 5 pixels/mm to 2 pixels/mm; (2) the image was output to a bitmap file; (3) this bitmap file was imported into the program Corelog, a program specifically designed to analyze CoreScan images; (4) several reference parameters (start depth, end depth, core diameter, sampling density) were input; and (5) bedding features were selected, by picking three or more points along the bed boundary, fitting a sinusoid to these picks, and if necessary modifying this solution. All bedding azimuths are with respect to an arbitrary reference (left margin of the image).

Based on the reliability with which each bedding horizon can be recognized and picked, it is classified as either dubious or fair/good. Of the 889 total bedding picks, 90% were classified as fair/good, but dubious picks were locally abundant enough to warrant their retention.

A wide variety of sedimentary structures, both depositional and post-depositional, is evident in the CRP-2A cores (Passchier, this volume) and whole-core images (Fig. 1). Soft-sediment deformation is common, particularly in the bottom part of the hole (Passchier, this volume); this deformation may be induced by either marine slumping or glacial loading. Lonestones affect local dip, both by loading of underlying sediments and by drape of overlying sediments. Laminated bedding (Powell & Claps, this volume) and cross bedding are locally evident. Because our focus is on delineation of primary and structural dips, we excluded soft-sediment deformation and lonestone sag and drape from our bedding picks. However, both can occur at a scale large enough to be missed in the core images. For example, we did not pick bedding within or immediately adjacent to observable soft-sediment deformation, but bedding a few centimeters away from such a zone was picked and could be affected either by drape or by slumping.

DIPMETER DATA PROCESSING

CRP-2/2A was logged with an Antares 4-pad, slimhole dipmeter. This tool measures conductivity at each pad at a 5-mm vertical spacing. CRP-2/2A was logged in two phases: the open-hole interval 166-65 mbsf was logged at the conclusion of HQ (96 mm hole diameter, 61 mm core diameter) drilling, then the interval 622-200 mbsf was logged at the conclusion of NQ (76 mm hole diameter, 45 mm core diameter) drilling. A repeat log was obtained for the interval 623-575 mbsf. Problems with tool electronics caused frequent failures of the data acquisition process during the second phase of logging. Consequently, the dipmeter log for the interval 622-200 mbsf consisted of 29 files, of varying length.

The dipmeter tool also records azimuth and angle of borehole deviation. CRP-2A was nearly vertical: deviation angle ranged from 0.3° to 1.1°, with an eastward deviation azimuth in the upper part of the hole and NW azimuth in the bottom portion. Although this deviation is minor, dipmeter dips are corrected from borehole to *in situ* coordinates. Core dips, in contrast, cannot be corrected because the cores are not oriented.

The Antares dipmeter uses a 3-axis magnetometer for azimuthal orientation. At the drillsite, magnetic inclination is nearly vertical (82°), resulting in only a small horizontal component for azimuthal orientation. Magnetic orientation at high latitudes can be a problem, because declinations there change dramatically in response to magnetic storms. Consequently, we used a portable 3-axis magnetometer as a reference, placing it on the ice about 30 m from the rig site, far enough away from the rig to avoid influence of the
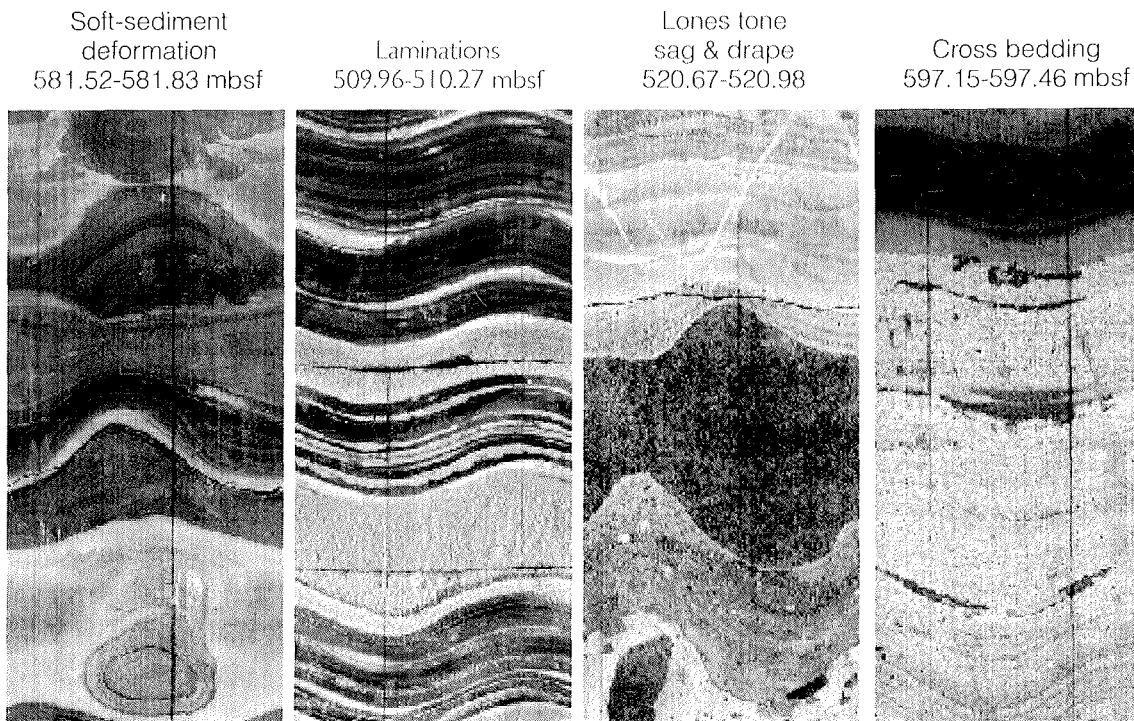
Soft-sediment
deformation   Laminations
581.52-581.83 mbsf   509.96-510.27 mbsf

Lones tone
sag & drape   Cross bedding
520.67-520.98   597.15-597.46 mbsf

Fig. 1 - Processes affecting CRP-2 bedding dips are illustrated in these four core images. Each image is an unwrapped 360° scan of the outer core surface, so planar features are evident as sinusoids. Soft-sediment deformation (left image) and lonestones (dark patches at the center and bottom of the third image) are generally non-planar and therefore non-sinusoidal in these scans. The two vertical lines in each image are reference lines drawn on the core.

rig steel on the magnetometer. This reference magnetometer recorded magnetic measurements every 5 seconds throughout the two phases of logging. Fortunately, magnetic activity was quiet during these two logging phases, with variations in local declination of <0.5°. Local deviation, the angle between true North and magnetic North, was measured with GPS surveys in August and October 1999. These measurements, 148.5° and 147.5°, are nearly identical to the predicted value of 148.3° at this location based on the International Geomagnetic Reference Field (IGRF). This remarkably high angle is a consequence of the rig site being at a higher latitude than that of the south magnetic pole. An average local deviation of 148° is assumed for all dipmeter analyses, as well as for conversion of borehole televiewer orientations from magnetic to geographic coordinates (Moos et al., this volume) and for core orienting (Paulsen et al., this volume).

Our first dipmeter processing step was to merge the 30 original dipmeter data files into a small number of files for further processing. As part of this step, conductivity readings for each pad were gain adjusted. The Antares tool uses a dynamic gain modification during logging, selecting an appropriate gain at each depth and recording both gain and reading. Our reprocessing converted all conductivities to a common gain.

In most sedimentary sequences, conductivity is an excellent parameter to measure for dip determination, because conductivity responds to changes in both porosity and lithology, and because the conductivities of porous rocks vary by more than 5 orders of magnitude. In CRP, however, a microconductivity-based dipmeter tool also responds to several variables other than bedding: fractures (open or cemented), patchy cements, and lonestones. Both carbonate nodules and lonestones are highly resistive,

creating spikes to low conductivity on one or more of the four pads. When dipmeter processing correlates the four pad signals in an attempt to identify the highest correlation and its associated dip, these spikes can easily dominate the correlation and generate spurious dips.

Figure 2 is an example of dipmeter data from a lonestone-rich interval, showing results from two of the four pads. The spiky character and poor correlation between adjacent pads are evident. Spikes to low conductivity occur throughout the CRP-2A dipmeter data, particularly below 350 mbsf. Zones with greatest spike abundance correlate with zones of high lonestone abundance, as inferred from spikiness of whole-core physical properties datasets (velocity, density, and magnetic susceptibility) (Cape Roberts Science Team, 1999; Niessen et al., this volume) and confirmed by lonestone counts (Cape Roberts Science Team, 1999; Brink et al., this volume)

To minimize the effects of lonestones and patchy cements on our dipmeter analyses, we employed two methods of spike removal. We subjectively edited all raw microconductivity traces, deleting spikes to low conductivity. We also developed an objective spike detection algorithm, which calculates the median of a 0.1 m interval of the four conductivity traces for each depth, then deletes data that are less than 75% of this median. This comparison to the median is quite effective for spike detection when the spike only affects one of the four pads, as is the case for the majority of lonestones [see, for example, the determinations of lonestone size distribution by Brink et al. (1998)], but some influence of larger lonestones slips through. An additional algorithm, to delete the flanks of detected spikes, was then applied to both datasets, subjective and objective. Finally, the gaps were filled by linear interpolation. Figure 2 compares raw and despiked data for
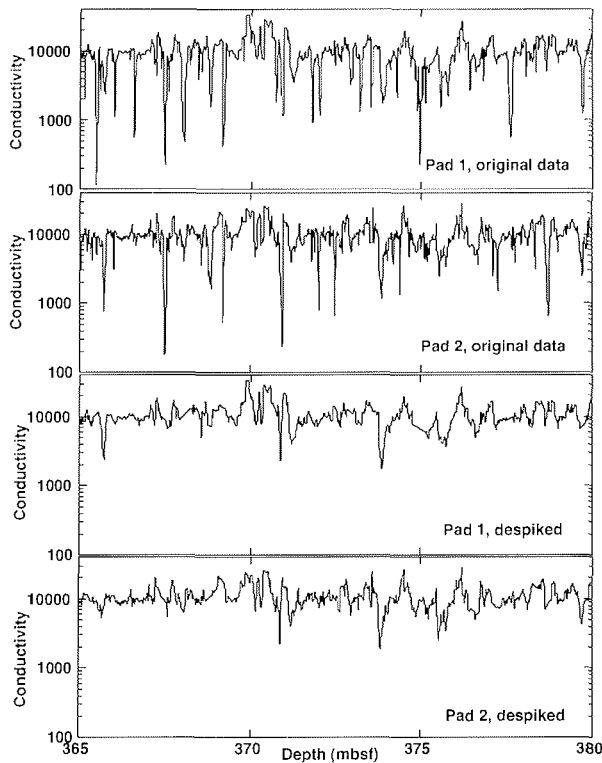
Fig. 2 - Short intervals from two of the four microconductivity traces recorded by the dipmeter. Lonestones cause frequent spikes to low conductivity. Because most lonestones are too small to be detected on more than one pad, they degrade trace coherence among pads. Application of a despiking algorithm (bottom two traces) minimizes this problem and improves reliability of correlations.

the lonestone-rich interval 365-380 mbsf.

Despiked logs from the four pads were combined to generate a single microconductivity log. We used the subjectively despiked logs rather than raw logs to minimize the biasing effect of lonestones. Each lonestone has a conductivity at least an order of magnitude lower than that of the surrounding porous sediments. Consequently, averaging lonestone data with lonestone-free data from the same depth gives an estimate that is much lower than the true net conductivity at that depth. Using the median provides a more representative estimate of *in situ* conductivity. This microconductivity log has similar low-frequency character to the lower-resolution induction log (Brink & Jarrard, this volume). Brink & Jarrard (this volume) convert both logs to porosity, and Brink et al. (this volume) present a sedimentological interpretation of both.

For processing of the despiked dipmeter data to determine bedding dips, we used the program Ezdip. Results depend on a variety of user-determined processing parameters. In an attempt to maximize signal-to-noise ratio, we experimented with various processing parameters, using as a ground truth the known variations in bedding dip as observed in several stitched core intervals. A window length of 0.25 m and step increment of 0.1 m were used. A correlation angle of 0-45° was used to encompass the range of bedding dips observed in cores, while minimizing accidental picking on fractures.

Ezdip uses an artificial intelligence algorithm to suppress inconsistent results (Kerzner, 1983, 1986, 1988). Because of this algorithm and use of a step increment

shorter than the window length, adjacent values are not independent. This lack of independence has two noteworthy impacts. First, confidence limits for averaged zonal dips are optimistic, because they assume independent data. Second, consistency of results over a several metre interval does not necessarily establish reliability of their pattern. Indeed, subtle changes in a processing parameter sometimes changed the entire pattern of dips within a 0.5-3 m interval. To evaluate and eliminate these zones with unstable solutions, we generated two alternative processing runs in addition to the final main run. One of these alternatives used the same processing parameters but used the dataset resulting from subjective, rather than objective, spike detection. The second alternative used a seemingly trivial change in step increment, 0.11 m instead of 0.1 m. We deleted dip determinations in any zone that exhibited substantial discrepancies among these three runs. Application of this stability criterion resulted in deletion of 10% of the results, from a total of 14 zones that were 0.1-11.2 m in length. A total of 1761 dip determinations survived this stability criterion.

Dipmeter analysis is also capable of detecting fractures. In an attempt to detect open and filled fractures within the CRP-2A dipmeter data, we employed processing parameters quite different from those used for bedding. For example, scan angle was increased to 85° and the requirement for planarity of results was relaxed. It is to be expected that results with dips of <45° would consist of a mixture of bedding and fractures, so these results were excluded. Unfortunately, results for dip angles of 50-85° exhibited near-random azimuths, except for a possible N-S fabric above 165 mbsf. We conclude that fractures were not identified with sufficient accuracy to be useful.

CORE RESULTS

Figure 3 plots all bedding dips based on picks from whole-core images. It should be noted that dips of <5° are underrepresented because of a detection bias. Most of the whole-core images exhibit some horizontal striping due to scan-line inhomogeneity, scan edge illumination variations, and sediment smearing on the rollers that hold the core. These artifacts make it difficult to detect bedding with dips of <5°.

Dip scatter at most depths is surprisingly high (Fig. 3). This scatter is real, as it is much larger than the sinusoid picking uncertainty of <3° based on replicate picks. This scatter is also higher than is typical for marine sediments; for example, the angle of repose for subaqueous sands is only a few degrees. We hypothesize that dip dispersion is increased in this glacial sedimentary environment by a variety of factors that are not obvious at the scale of individual decimeter-to-millimeter beds. Sedimentary processes include sag and drape associated with large lonestones that are adjacent to, but do not intersect, the borehole. Drape over non-horizontal slump surfaces and terminal moraines may also occur. Post-depositional deformation is probably common in these sediments, particularly associated with the glacial scour and loading events which are thought to have been abundant (Cape Roberts Science Team, 1999). Consequently, soft sediment deformation is probably more pervasive than was evident in the cores. One indication of this unobserved soft-
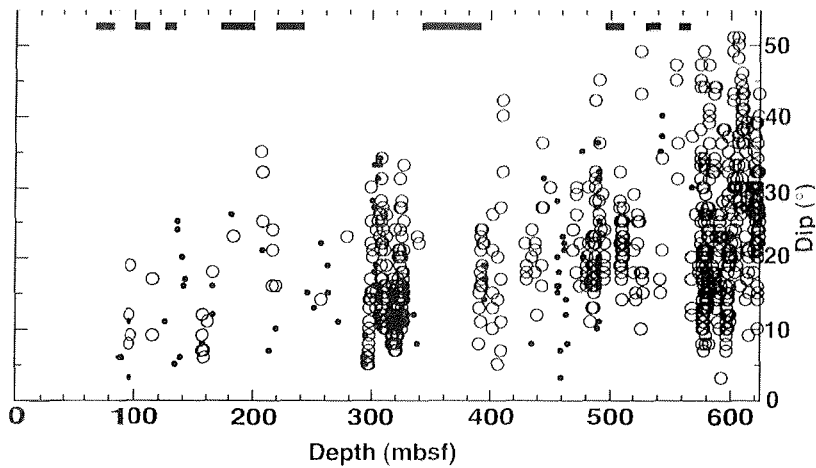
Fig. 3 - Identifications of bedding dip on whole-core scan images. Open circles are picks classified as fair/good; solid dots are dubious picks. Solid vertical bars indicate intervals that were not analyzed. Note the high dip dispersion and the gradual increase in dips downhole.

sediment deformation is the particularly high dispersion in the bottom 100 m, where soft-sediment deformation was most commonly noticed and avoided. A related indication is the higher dispersion in steeply dipping intervals than in nearby subhorizontal zones.

Downcore trends in dip magnitude are discussed in a later section on implications for tectonic history.

Dip azimuths of these unoriented cores are not shown or considered here. Within stitched cores, azimuths are generally highly consistent. Paulsen et al. (this volume) use these core dip azimuths, along with dipmeter-based azimuths from the next section, to orient some of the cores.

DIPMETER RESULTS

Figure 4 is a histogram of dip azimuths for the 1761 dipmeter bedding determinations. A strong peaking at a modal azimuth of 82° is evident. This dip direction is reasonably consistent with the 75° dip direction based on a seismically determined structure contour map around CRP (Cape Roberts Science Team, 1998).

Not all dip azimuths in Figure 4 are to the east. In part, this azimuth dispersion is attributable to noise. When average dip magnitude is less than dip dispersion (e.g., circular standard deviation), all azimuths are represented, and our average dips of <15° are often less than the standard deviation of measurements. This noise is minimized by considering interval means, with associated 95% confidence limits, rather than individual data points. Some variation of azimuth from the 82° mode is real. For example, the distribution in Figure 4 is skewed, suggesting that NE dips are more common that SE dips. This variation, too, is best investigated by considering interval means.

Interval means are calculated by applying Fisher statistics, applicable to dispersion on a sphere, to the poles to bedding. This method is superior to the separate arithmetic averaging of dip directions and dip azimuths, particularly for small dips. For example, random errors superimposed on a mean bedding dip of 0° may generate apparent dips of 0-20° and an average dip of 10°, whereas Fisher statistics will correctly determine the mean dip as near zero. Another common approach to dipmeter analysis is to examine patterns within so-called "tadpole plots", dip vs. depth plots in which dip azimuth is indicated by a short line segment on each data point.

For CRP-2A, we have examined both tadpole plots and stereographic plots of poles to bedding, to extract any systematic dip patterns that may be present. Because of the quantity of data, however, we display only the results from interval means. The selection of intervals and their boundaries is based primarily on identification of sudden changes in average dip direction (dip magnitude or azimuth) on the tadpole and stereographic plots. A secondary criterion is to divide intervals bracketing significant data gaps (e.g., between logging phases 1 and 2, or in zones with insufficient conductivity character or coherence for dip determination). Finally, several intervals exhibited such an abundance of dips (>140 determinations) that they could be split to detect subtler depth-dependent variations, without unduly increasing confidence limits.

Table 2 lists results for the 31 uniform-dip intervals defined by CRP-2A dipmeter variations, and figure 5 plots the interval means with associated 95% confidence circles. As previously mentioned, these confidence circles are optimistically small, because adjacent data points are not truly independent. The size of 95% confidence circles is dependent on two parameters, data dispersion and number of points, and their relative importance is not evident in figure 5. We note that data dispersion was generally high above 150 mbsf, and very low below 480 mbsf.

Five of the 31 uniform-dip intervals are clearly anomalous, both on the tadpole plot and stereographic plot, when compared to adjacent intervals (Tab. 2). All
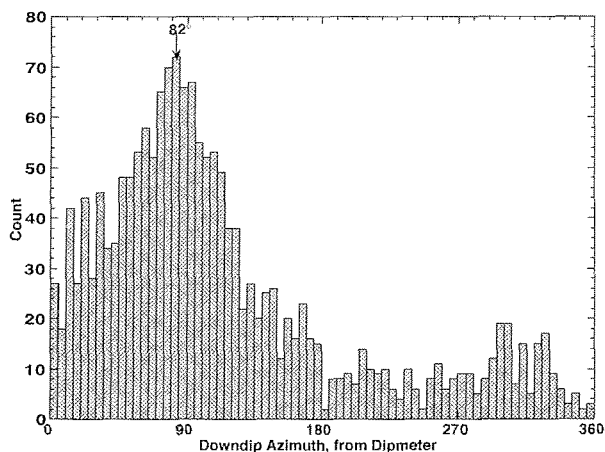

Fig. 4 - Histogram of all downdip azimuths determined by dipmeter. The strong peaking at 82° is attributable mainly to structural dip.

Tab. 2 - Average dip directions from intervals of dipmeter log.

Interval ID Label	Start Depth (mbsf)	End Depth (mbsf)	Downdip Azimuth	Dip (°)	Eastward Tilt (°)	# Points	95% Conf. Limits
A	65.0	81.9	316.6	11.7	-5.5	48	5.7
	82.8	88.1	78.9	4.6		15	11.8
B	88.1	101.3	268.5	7.3	-7.1	49	5.3
C	103.5	109.1	307.8	14.7	-8.8	21	6.1
D	109.5	137.4	146.5	2.8	0.9	81	4.3
E	145.4	152.0	37.2	14.0	11.0	32	4.2
F	152.1	159.9	96.2	9.2	8.6	53	2.6
	160.0	160.9	336.0	13.1		10	2.7
G	161.3	165.0	83.5	12.9	12.8	20	4.7
H	200.5	209.8	355.7	13.3	2.4	35	4.6
I	209.9	229.8	74.0	9.9	9.9	50	3.7
J	241.1	254.2	117.2	3.9	2.9	74	3.4
K	280.7	296.5	67.5	6.2	6.1	86	2.6
L	299.0	322.3	89.2	8.4	8.1	101	2.0
M	322.5	348.0	91.7	13.8	13.2	127	2.1
N	359.4	368.9	92.7	16.0	15.2	19	5.3
O	380.5	401.4	146.8	5.9	1.8	98	2.9
P	401.5	408.7	15.6	8.7	4.4	45	2.3
	409.0	412.6	296.7	13.5		16	6.4
Q	420.9	433.9	66.7	6.4	6.3	86	2.8
R	435.2	458.5	81.4	12.6	12.5	44	3.5
S	461.6	479.6	92.6	2.4	2.3	48	3.4
T	480.7	506.9	77.7	16.0	16.0	136	2.4
U	507.5	516.2	77.0	21.0	21.0	87	2.2
V	520.8	536.4	67.6	12.7	12.6	68	3.1
	540.5	544.0	283.4	9.9		10	8.6
W	545.9	559.2	64.6	16.4	16.1	28	3.5
	560.1	564.4	56.3	9.8		9	14.0
X	567.1	581.9	65.2	13.6	13.4	76	3.2
Y	584.8	600.8	54.1	14.7	13.7	136	2.7
Z	612.1	621.8	59.8	17.0	16.4	53	4.2

five are very short (0.8-5.3 m), and it is likely that dips of these zones are responding more to depositional processes (e.g., cross-bedding) or soft-sediment deformation than to structural dip. Consequently, we exclude these intervals from subsequent interpretations of structural dip variations. These five intervals are anomalous only in the sense of divergence from nearby dip patterns. Their large confidence circles result from paucity of points and do not indicate high data dispersion. As shown in figure 5, all have dip directions that are also observed in much longer intervals elsewhere in the stratigraphic section.

IMPLICATIONS FOR TECTONIC HISTORY

Based on seismic surveys in the vicinity of CRP (Cooper et al., 1987; Hamilton et al., 1998), an average structural dip of about 2-5° to the east is expected for CRP-2A (Cape Roberts Science Team, 1999). Sedimentological and palaeontological correlations between the Miocene sections at CRP-1 and 2 (Cape Roberts Science Team, 1999) similarly suggest an eastward dip of about 5°. Hamilton et al. (1998) identified an onlap sequence boundary in the regional seismic data, and preliminary CRP-2A depth-to-time conversion indicated that this expected angular unconformity is at a depth of about 83-215 mbsf in CRP-2A (Cape Roberts Science Team, 1999). Revised time-to-depth conversion of the seismic line crossing CRP-2A indicates that dips steepen from about 3° to 13° downhole (Henrys et al., this volume).

Although depth-dependent variations in dip can be identified in the stereographic plots of figure 5, a plot of dip vs. depth may be more useful for this purpose. For structural interpretation, however, total dip is less relevant than dip in the 75° plane of structural tilting. Consequently, for each dipmeter interval mean, we calculated and plotted the component of dip within this structural tilt plane; this value is equivalent to 90° minus the distance from the pole of a bedding set to a point with 0° dip and 255° azimuth. Figure 6 shows these dipmeter-based estimates of tilt vs. depth. Positive values indicate "eastward" (actually towards 75°) tilt, and negative values indicate "westward" tilt.

Dipmeter (Figs. 5 & 6) and whole-core imaging (Fig. 3) dip results agree in indicating a gradual downhole increase in dip within CRP-2A. Near the bottom of the hole, both give dips of 10-20°; dipmeter data below 480 mbsf provide an average dip estimate of 15±2°, similar to tentative seismic interpretations of Cape Roberts Science Team (1999). Core dips increase to 20-30° at the very bottom of the hole (605-625 mbsf) (Fig. 3), but this interval is short, soft-sediment deformation is locally evident, and dipmeter data do not provide confirmation (Fig. 6).

Dipmeter data indicate structural dips of <10° above about 300 mbsf. Bedding is rarely observed in core images from above 295 mbsf, and half of this identified bedding is classified as dubious (solid dots on Fig.3). Observed core dips above 295 mbsf are scattered, generally with values of 5-25°. Because of this high dispersion and because core dips of <5° are usually obscured by horizontal image striping, these core data are incapable of testing the dipmeter result.

The three shallowest dipmeter results indicate dips of several degrees to the northwest. This pattern is unexpected, as all seismic dips are toward the east. The seismic data do
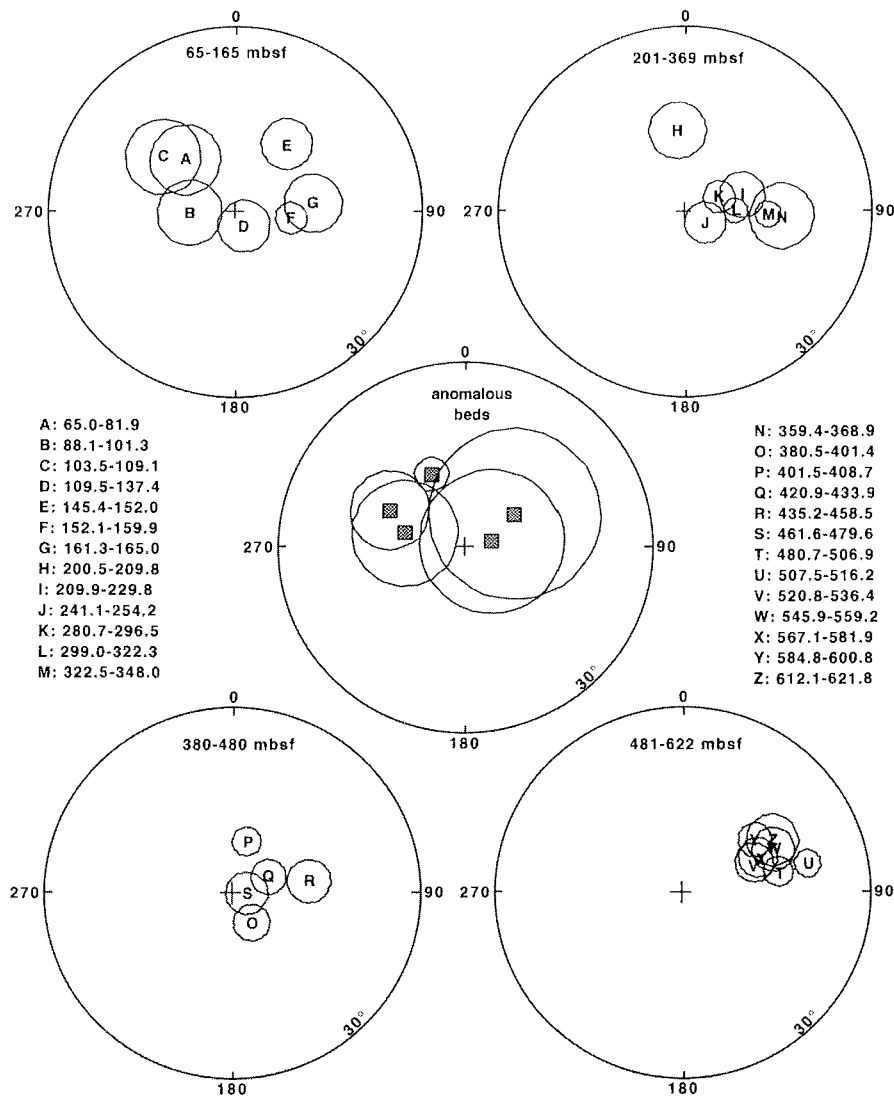
Fig. 5 - Mean dip directions (indicated by a letter or square) and associated 95% confidence circles for 31 depth intervals of CRP-2, based on dipmeter data. Results are listed in Table 2. In these zoomed stereographic projections, dip magnitude increases from zero at the center to 30° at the outer circle of each plot. Note the predominance of moderate eastward dips, as well as apparently systematic depth-dependent changes for some adjacent intervals. "Anomalous beds" are short depth intervals with directions discrepant from adjacent intervals, probably because of local sedimentary dips.

not preclude locally divergent dips, as seismic resolution is low and seismic reflectors are here caused by sequence boundaries rather than by bedding within sequences. Correlations between CRP-1 and CRP-2/2A (Cape Roberts Science Team, 1999) are consistent with seismic evidence, implying an eastward dip of 5° for this portion of CRP2. Unfortunately, the core data of figure 3 are unoriented and therefore incapable of distinguishing westward from eastward dips. The discrepancy between shallow dipmeter results and both seismic and interwell evidence, coupled with the high dispersion of dipmeter data for 65-150 mbsf, suggests that these unconfirmed dipmeter results should be treated with caution.

Superimposed on the dipmeter results of figure 6 are the dips of seismic reflectors that intersect the drill site (Henrys et al., this volume). In contrast to the substantial local dip variations implied by dipmeter data, seismic dips exhibit a smooth, gradual increase downhole. This difference cannot be attributed to dipmeter picking error, as dip inhomogeneity is confirmed by core images (Fig. 3). The large averaging volume of seismic profiling minimizes effects of sedimentary dip inhomogeneity, permitting

structural dip to dominate.

Are the core and log data capable of detecting variations in structural dip in more detail than the generalization of downhole dip increase? Perhaps, but not uniquely. Below we present two possible interpretations: sawtooth dip history, and angular changes at previously recognized unconformities.

SAWTOOTH DIP HISTORY

The dip variations of figure 6 appear to exhibit a sawtooth pattern, with three intervals of gradual downhole increase in eastward dip (65-165 mbsf, 200-369 mbsf, and 380-516 mbsf), separated by sudden jumps to lower or zero dip.

One possible mechanism for such a pattern is that episodic faulting generates eastward dip, followed by gradual sedimentary filling of the accommodation space and attendant dip reduction. That normal faulting is responsible for eastward dips is undoubted: regional seismic data clearly show that the tectonic history of the Western Ross Sea is one of normal faulting and associated major eastward thickening and deepening of sedimentary
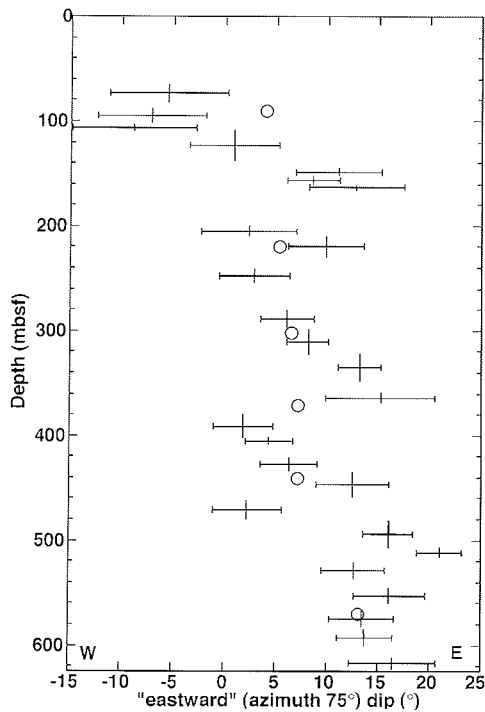
Fig. 6 - Mean dipmeter-based dip directions of figure 5 and table 2, displayed as a plot of "eastward" tilt versus time. These tilts are the dip component in the seismically determined structural dip plane of 75° azimuth. Vertical bars indicate depth range for which data are combined, and horizontal bars are 95% confidence limits from table 2. Observed downhole variations result from a combination of structural tilting and local sedimentary dips. Open circles: dips of seismic reflectors at CRP-2A, from Henrys et al. (this volume).

sequences (Cooper et al., 1987). However, neither the sedimentary facies nor sequence stratigraphy of CRP-2A (Cape Roberts Science Team, 1999; Fielding et al., this volume) indicates that the intervals 65-165, 300-369, and 380-516 mbsf are shallowing-upward packets. Furthermore, this scenario implies a systematic downhole increase of dips among the three packets, but such an increase is not observed.

Another possible mechanism for a sawtooth dip pattern is activity on two normal faults on opposite sides of the site: an episodic fault and a continuous growth fault. Again, however, such a tectonic history is expected to impact sedimentary facies, water depths, sequence stratigraphy, and biostratigraphic unconformities at CRP-2A. This predicted association is not observed.

ANGULAR CHANGES AT PREVIOUSLY RECOGNIZED UNCONFORMITIES

CRP-2A appears to consist of about 25 sequences, based on either core analysis (Cape Roberts Science Team, 1999; Fielding et al., this volume) or log analysis (Brink et al., this volume). Any sequence boundary may have an associated unconformity, but three major unconformities are hypothesized on the basis of biostratigraphic and other age data: 130 mbsf, 306 mbsf, and about 440 mbsf (Cape Roberts Science Team, 1999). Based on lithologic and well-log variations between these unconformities, Brink et al. (this volume) suggest that they may bound fining-upward sequence sets. Can dipmeter and core dips detect angular unconformities at these locations?

The 130 mbsf unconformity occurs within interval D of figure 5 and table 2. Interval D is a transition interval, from apparent NW dips in overlying intervals A-C to eastward dips in all underlying intervals. The dipmeter data are therefore compatible with interpretation of the 130 mbsf unconformity as an angular unconformity, with about a 15° change in dip across the boundary. As previously discussed, however, the dipmeter indication of NW dips above 130 mbsf is inconsistent with both seismic and interwell evidence.

A major unconformity that is seen at about 306 mbsf in cores (Cape Roberts Science Team, 1999) is not evident as an angular unconformity in the dipmeter data. Instead, the interval 241-369 mbsf appears to exhibit a gradual increase in dip (Tab. 2, Figs. 5 & 6). These data do not exclude the possibility of a <5° angular unconformity near 300 mbsf. To test this possibility in more detail, we examined all whole-core scans for 240-340 mbsf in an effort to pick dips of all observable bed boundaries. Figure 3 shows these results in the context of overall dip variations within CRP-2A, and figure 7 examines dip variations within the interval 200-340 mbsf. A sudden downcore increase in dip, from 5-10° to 10-30°, may indeed be present. The increase occurs at 297 mbsf rather than at 306 mbsf. Presence of this possible angular unconformity, however, is based primarily on the tight cluster of laminated beds at 295-297 mbsf. Above 295 mbsf, few bedding horizons are evident in the cores, and their dips are scattered and >10°.

The 440 mbsf boundary between sequence sets marks a major shallowing of water depth (Cape Roberts Science Team, 1999; Brink et al., this volume) and a last occurrence for several diatom taxa (Scherer et al., this volume). Dipmeter data demonstrate that the bottom portion of CRP-2A, below 481 mbsf, exhibits remarkably constant dip orientations (Fig. 5), despite common soft-sediment deformation. The structural top of this unit may be as deep as 481 mbsf or as shallow as 435 mbsf: interval R gives a result indistinguishable from those of the deeper T-Z intervals, but underlying interval S is discrepant (Fig. 5). If interval S is nonrepresentative of structural dip because of either primary or post-depositional processes, then bracketing data may indicate an angular unconformity near the 440 mbsf sequence-set boundary. Although every whole-core image between 400 and 500 mbsf was examined, no angular unconformity is evident within this interval (Fig. 8).
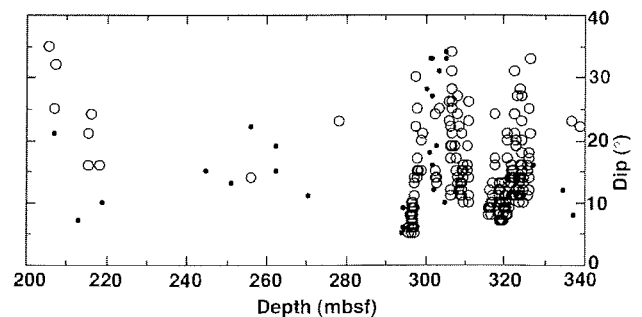

Fig. 7 - A portion of the whole-core bedding dip dataset of figure 3, displaying the interval 200-340 mbsf. These data are compatible with the hypothesis of an angular unconformity at about 300 mbsf, but they are inconclusive.
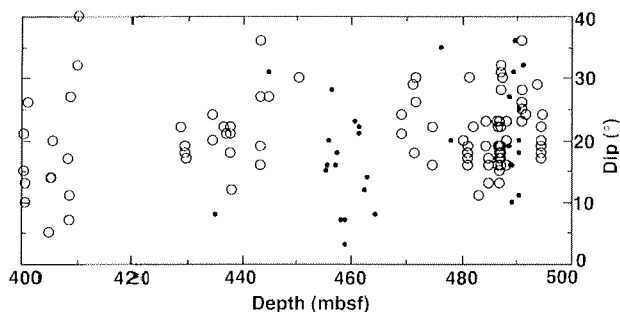
Fig. 8 - A portion of the whole-core bedding dip dataset of figure 3, displaying the interval 400-500 mbsf. These data do not confirm dipmeter-based evidence of an angular unconformity within the interval 440-479 mbsf.

SEDIMENTARY DIPS

Patterns of systematically changing bedding dip, whether observed in outcrop or in dipmeter data, are often interpretable in terms of sedimentary facies. Whole-core images have a similar potential. We have not undertaken such an interpretation for the whole-core images from CRP-2A, despite their rich record of sedimentary facies information, because the cores are not oriented. Instead, we concentrate below on evidence from dipmeter data.

In previous sections, the dipmeter dataset has been subdivided into zones based entirely on consistency of dip directions. Alternatively, one can subdivide these data by lithology or by systems tract. CRP-2A core lithologies were described by Cape Roberts Science Team (1999). A sequence stratigraphic model has been applied to CRP-2A cores (Cape Roberts Science Team, 1999: Fielding et al., this volume) and logs (Brink et al., this volume), dividing CRP-2A into two dozen sequences. Core and log sequences have been further subdivided into systems tracts (lowstand, transgressive, highstand, and regressive), thought to reflect changes in sea level and/or glacial processes. These complementary approaches yield generally very close agreement (Brink et al., this volume). We use the log-based systems tracts rather than core-based ones, because only the former identify locations of lowstand/transgressive and highstand/regressive systems tract boundaries.

Mean dip directions for lithologically defined beds or units are shown in figure 9A, and means for individual systems tracts are shown in figure 9B. Only intervals with at least 6 dip determinations and with 95% confidence limits of less than 14° are included; confidence limits for most intervals are <6°. To isolate any possible sedimentary dips from structural dip, we have removed structural dips. An approximate structural dip correction, estimated from the seismic dips and average dipmeter dips of figure 6, is 2° plus 2° per 100 m, along an azimuth of 75° E.

No CRP-2A lithology has dip directions that diverge systematically from other lithologies (Fig. 9A). This result is surprising, as one might expect more sedimentary dip variations and generally steeper dips among the diamict-dominated units than in the deeper-water muds and mixed muds and sands. The primary mechanism of initial sedimentation for these diamicts is at the toe of glaciers, forming submarine terminal moraines (Cape Roberts Science Team, 1999; Powell, this volume). These sediments are readily remobilized, however, as glacigenic sediment flows. Lonestone fabric analyses indicate weak fabrics

within the diamicts, suggestive of sediment flows rather than lodgment or meltout till (Cape Roberts Science Team, 1999). Moraines can have significantly steeper internal dips than offshore hemipelagic sediments, whereas sediment flows and lodgment till can have dips approximately parallel to the underlying sea floor. The latter is more consistent with our observation of no detectable dependence of mean sedimentary dips on lithology.

No systematic pattern of dip differences is observed among lowstand, transgressive, highstand, and regressive systems tracts (Fig. 9B). This result appears to be inconsistent with a scenario in which submarine topography is created by generation of terminal moraines during lowstands, then gradually removed by drape during subsequent transgressive and highstand sedimentation. Again, redeposition may obscure such a pattern.

Possible lithologic effects on dip can also be investigated via histograms of dipmeter-based downdip azimuths, with diamict-dominated lithologies plotted separately from sands and muds (Fig. 10). Data from conglomerates, conglomeratic sands, large lonestones, a thick ash layer, and unknown lithology (no core recovery) are excluded from figure 10. Azimuths for conglomerates, large lonestones, and no core recovery are similar to the overall averages of figures 10 and 4, whereas the azimuths of sandy conglomerates are skewed
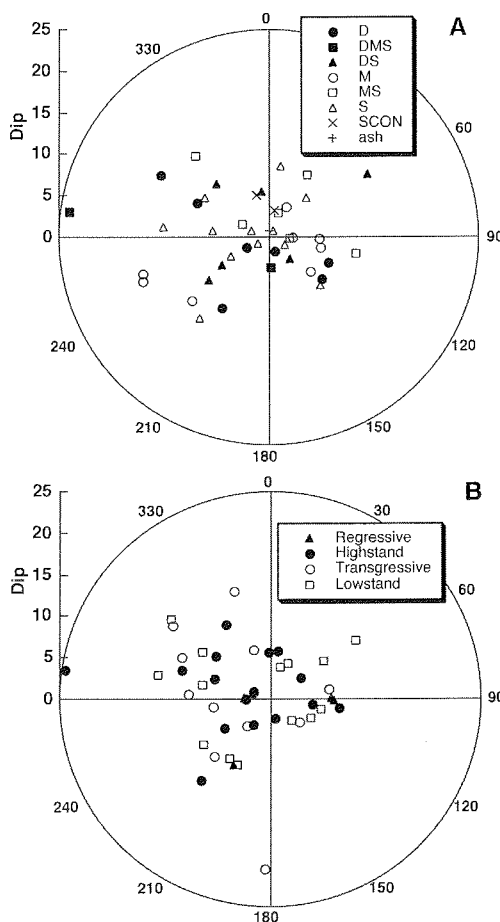

Fig. 9 - A: Mean dipmeter-based dip directions for intervals of uniform lithology. Solid symbols: diamict-dominated lithologies (D: diamict; DMS: mixed diamict, sand, and mud; DS: mixed lonestone-rich sand and diamict); open symbols: sands and muds (M: muds; MS: mixed muds and sands; S: sands); SCON: conglomeratic sands. B: mean dip directions for individual systems tracts (regressive, highstand, transgressive, or lowstand). All dip directions are rotated to remove structural dip.
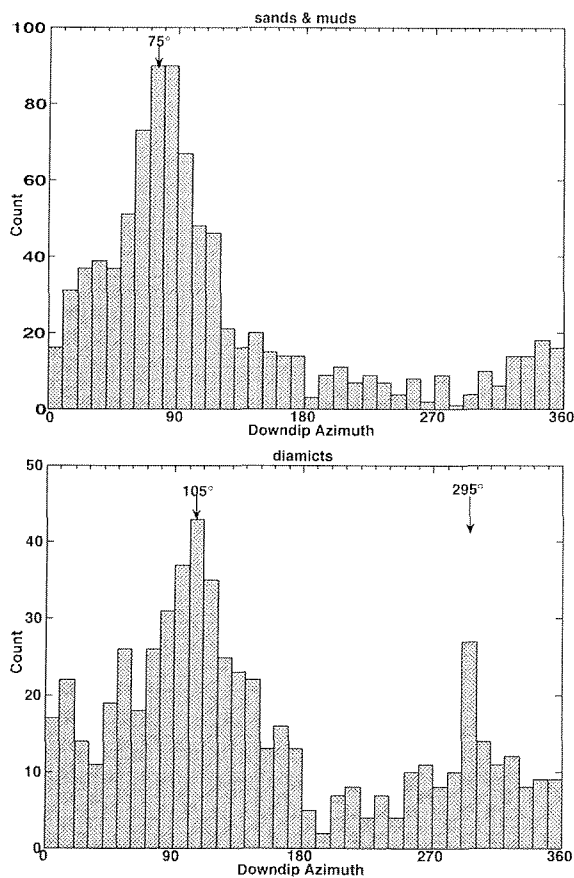
Fig. 10 - Histograms of downdip azimuths determined by dipmeter. Data for sands and muds (top) are plotted separately from those for diamict-dominated lithologies (bottom).

slightly toward the northeast, and azimuths within the ash layer are almost random.

In contrast to the results from interval means, azimuths of individual dip determinations do appear to detect a lithologic effect on dip direction (Fig. 10). Sands and muds exhibit a strong and symmetrical peak at a mean azimuth of 74° and median azimuth of 76°. Diamict azimuths have a higher variation, with a main peak centered at 105° and with a small secondary peak at about 295°.

We tentatively interpret these two azimuth patterns as indicating sedimentary dip differences that are too subtle to be detected in the interval means of figure 9. If the sands and muds were deposited on a shelf which – like most modern continental shelves – is within a degree of horizontal, then they provide our best estimate of structural dip. Muds are expected to have less variance associated with primary sedimentary dips than sands, but separate histograms for CRP-2A muds, sands, and mixed sands and muds are nearly identical. This 74°-76° average azimuth for sands and muds more closely matches the seismically determined downdip azimuth of 75° than does the 82° average of all lithologies (Fig. 4).

Glacial advance probably was not parallel to shelf and structural dip, but ESE or SE, away from its Granite Harbour source (Cape Roberts Science Team, 1998, 1999). Accordingly, diamict dip azimuths are ESE, about 30° different from sand and mud dip azimuths. NNE-trending terminal moraines at the looming glacial front would generate sediment flows predominantly to the ESE. During glacial retreat, however, the terminal moraine loses relief by sediment flows to both the ESE and WNW, and this process may be responsible for the secondary azimuth peak at 295°, 190° from the dominant diamict azimuth.

CONCLUSIONS

Bedding dips at CRP-2A exhibit a high dispersion, due to a combination of depositional and postdepositional processes, that overprints the signal from structural tilting. Whole-core images and dipmeter results concur in indicating a downhole dip increase, to about 15° in the bottom 150 m. Both also suggest that about 5-7° of this dip increase occurs in the interval 320-480 mbsf. The extent to which finer-scale variations in structural dip can be extracted from these data is, however, debatable.

The highly consistent dip results below 481 mbsf (Fig. 5), indicating a structural dip of 15±2° (Fig. 6), have implications for the siting of CRP-3. Current plans are for CRP-3 to be located 2.2 km west of CRP-2A. Based on a preliminary time-to-depth conversion of the seismic line connecting these sites, it is expected that a seismic reflector about 50 m from the bottom of CRP-2A will intersect CRP-3 about 35 m from its top (Cape Roberts Science Team, 1999). If CRP-3, like CRP-2A, has about 30 m of unconsolidated sediments overlying the older, target section, then a 50 m overlapping section at the two sites is anticipated. However, the seismic reflector anchoring this projection indicates 13° dip near the base of CRP-2A. If, as indicated by the data of this study, dips are 15° in the lower part of CRP-2A, then velocities are slightly higher than assumed in the seismic time-to-depth conversion and the expected overlap zone vanishes. A slight reduction in site spacing may be needed, to assure that overlapping sections will be obtained.

REFERENCES

Brink J.D., Jarrard R.D., Krissek L.A. & Wilson T.J., 1998. Lonestone abundance and size variations in CRP-1 drillhole, Victoria Land Basin, Antarctica, *Terra Antartica*, **5**(3), 367-374.

Cape Roberts Science Team, 1998. Initial Report on CRP-1, Cape Roberts Project, Antarctica. *Terra Antartica*, **5**(1), 187 pp.

Cape Roberts Science Team, 1999. Studies from the Cape Roberts Project, Ross Sea, Antarctica, Initial Report on CRP-2/2A. *Terra Antartica*, **6**(1/2), 173 pp.

Cooper A.K., Davey F.J. & Behrendt J.C., 1987. Seismic stratigraphy and structure of the Victoria Land Basin, Western Ross Sea, Antarctica. In: Cooper A.K. & Davey F.J. (eds.), *The Antarctic Continental Margin: Geology and Geophysics of the Western Ross Sea, Circum-Pacific Council for Energy & Mineral Resources Earth Science Series*, **5B**, Houston TX, 27-75.

Hamilton R.J., Sorlien C.C., Luyendyk B.P., Bartek L.R. & Henrys S.A., 1998. Tectonic regimes and structural trends off Cape Roberts, Antarctica, *Terra Antartica*, **5**(3), 261-272.

Kerzner M.G., 1983. Formation dip determination – an artificial intelligence approach. *Log Analyst*, **24**(5), 10-22.

Kerzner M.G., 1986. *Image Processing in Well Log Analysis*, IHRDC, Boston.

Kerzner M.G., 1988. A rule-based approach to dipmeter processing, *SPE*, paper 18128.